

---

---

# DNA Damage in Peripheral Blood Lymphocytes of Thyroid Cancer Patients After Radioiodine Therapy

Uta Eberlein\*<sup>1</sup>, Harry Scherthan\*<sup>2</sup>, Christina Bluemel<sup>1</sup>, Michel Peper<sup>2</sup>, Constantin Lapa<sup>1</sup>, Andreas Konrad Buck<sup>1</sup>, Matthias Port<sup>2</sup>, and Michael Lassmann<sup>1</sup>

<sup>1</sup>Department of Nuclear Medicine, University of Würzburg, Germany; and <sup>2</sup>Bundeswehr Institute of Radiobiology affiliated to the University of Ulm, Munich, Germany

---

The aim of the study was to investigate DNA double-strand break (DSB) formation and its correlation to the absorbed dose to the blood in patients with surgically treated differentiated thyroid cancer undergoing their first radioiodine therapy for remnant ablation. **Methods:** Twenty patients were included in this study. At least 7 peripheral blood samples were obtained before and between 0.5 and 120 h after administration of radioiodine. From the time-activity curves of the blood and the whole body, residence times for the blood self-irradiation and the irradiation from the whole body were determined. Peripheral blood lymphocytes were isolated, ethanol-fixed, and subjected to immunofluorescence staining for colocalizing  $\gamma$ -H2AX/53BP1 DSB-marking foci. The average number of DSB foci per cell per patient sample was analyzed as a function of the absorbed dose to the blood and compared with an in vitro calibration curve for <sup>131</sup>I and <sup>177</sup>Lu established previously in our institution. **Results:** The average number of radiation-induced foci (RIF) per cell increased over the first 3 h after radionuclide administration and decreased thereafter. A linear fit from 0 to 2 h as a function of the absorbed dose to the blood agreed with our in vitro calibration curve. At later time points, RIF numbers diminished, along with dropping dose rates, indicating progression of DNA repair. Individual patient data were characterized by a linear dose-dependent increase and a biexponential response function describing a fast and a slow repair component. **Conclusion:** With the experimental results and model calculations presented in this work, a dose-response relationship is demonstrated, and an analytic function describing the time course of the in vivo damage response after internal irradiation of patients with <sup>131</sup>I is established.

**Key Words:**  $\gamma$ -H2AX; 53BP1; biological dosimetry; radioiodine therapy; DTC; absorbed dose to blood; dose response; DSB focus assay; DNA damage; <sup>131</sup>I; differentiated thyroid cancer

**J Nucl Med 2016; 57:173–179**  
DOI: 10.2967/jnumed.115.164814

---

**A**fter total thyroidectomy for differentiated thyroid cancer (DTC), patients generally receive one or more treatments with high activities of <sup>131</sup>I. The purpose of the initial radioiodine therapy

after surgery is to ablate remnant thyroid tissue and to effectively treat any iodine-avid metastases (1,2). Because patients with DTC generally do not undergo chemotherapy or other radiotherapy before radioiodine therapy, this patient group is ideally suited for the investigation of the DNA damage in blood lymphocytes induced by protracted, nearly homogeneous whole-body irradiation. In this setting, all organs, including the blood, are irradiated by  $\beta$ -particles emitted from circulating <sup>131</sup>I and from penetrating  $\gamma$ -radiation originating from activity dispersed throughout the body. The absorbed dose and dose rate to the blood is assessed by defining the time-activity curves in the blood and the whole body, integrating the corresponding time-activity curves and calculating the absorbed dose according to European Association of Nuclear Medicine (EANM) standard operating procedure (SOP) for DTC (3).

Ionizing radiation not only destroys the malignant iodine-avid cells but also damages healthy tissues and cells. Among the elicited damage, DNA double-strand breaks (DSBs) are the most crucial lesions for the healthy tissue because their repair can be difficult, and faulty DNA repair leads to mutations, chromosomal aberrations, or cell death.

In general, DSBs evoke a DNA damage response during which the DSB signal is amplified and several repair routes are induced involving proteins that can serve as biomarkers (4).

The formation of a DSB in nuclear chromatin results in the rapid phosphorylation of the histone H2 variant H2AX, then called  $\gamma$ -H2AX (5–7). Furthermore, DSBs also recruit the damage sensor protein 53BP1 to the chromatin around DSBs (8–12), leading to 53BP1 and  $\gamma$ -H2AX colocalization in the chromatin surrounding a DSB (8,10,13–15). By immunofluorescence staining with  $\gamma$ -H2AX and 53BP1 antibodies those biomarkers can be addressed as microscopically visible fluorescent foci (14–16). With progression of DSB repair,  $\gamma$ -H2AX and 53BP1 foci disappear (17).

At present, there are only two studies that quantified radiation-induced DNA damage foci formation after therapy of DTC with the isotope <sup>131</sup>I, either using radiation-induced colocalizing  $\gamma$ -H2AX and 53BP1 foci (18) or using  $\gamma$ -H2AX foci alone (19). More recent studies addressed  $\gamma$ -H2AX foci formation after <sup>177</sup>Lu therapy of neuroendocrine tumors (16,20). In these studies the authors observed elevated levels of radiation-induced DNA damage foci after treatment, but a clear dose-response relationship could only be established in one study (16).

The aims of this study were therefore, to compare the in vivo dose response in the first hours after therapy with an in vitro calibration curve established recently in our laboratory (15), and to describe the temporal and dose-dependent behavior of the radiation-induced foci (RIF) in radiation treatment-naïve patients after their first radioiodine therapy (RIT).

---

Received Jul. 31, 2015; revision accepted Oct. 28, 2015.  
For correspondence or reprints contact: Michael Lassmann, Department of Nuclear Medicine, University Hospital Würzburg, Oberdürrbacher Strasse 6, 97080 Würzburg, Germany.  
E-mail: Lassmann\_m@ukw.de  
\*Contributed equally to this work.  
Published online Nov. 12, 2015.  
COPYRIGHT © 2016 by the Society of Nuclear Medicine and Molecular Imaging, Inc.

## MATERIALS AND METHODS

### Research Design and Subjects

Patients referred to our center for initial treatment with radioiodine after surgery for differentiated papillary or follicular thyroid carcinoma were included in this study. Before treatment, each patient received 3–8 MBq of  $^{131}\text{I}$  for thyroid bed tracer uptake measurement to screen for thyroid remnants large enough to require reoperation. Patients with a 24-h iodine uptake of more than 5% in the thyroid bed were excluded from the study. Higher uptake in the thyroid bed would affect the dosimetry calculations. No patient had a history of leukemia or lymphoma or radio- or chemotherapy and none underwent an x-ray examination or, other than the remnant tracer uptake measurement, scintigraphy within 3 mo before radioiodine therapy. The research plan was presented to the ethics committee of the Medical Faculty of the University of Würzburg (Az: 112/11). The ethics committee approved the study by stating that there were no objections to the conduct of the study. Before the study, all patients gave their written informed consent. For treatment, the patients were hospitalized for at least 48 h, normally up to 3–4 d.

### Blood Sampling and Activity Determination of Blood Samples

Blood samples were drawn in all patients before administration and nominally at 0.5, 1, 2, 3, 4, 24, 48, and up to 168 h after administration using Li-Heparin blood collecting tubes (S-Monovette). For an exact quantification of the blood activity concentration, an aliquot of 0.1 mL of each heparinized blood sample was measured in a well counter (Canberra) or in a high-purity germanium detector (Canberra). The counting efficiencies of both detectors were determined by repeated measurements of a National Institute of Standards and Technology–traceable standard. The measured values were decay-corrected to the time of blood drawing. The statistical error of the activity determination was less than 1% for the blood samples taken at the first day. The statistical error increased for later time points but was always less than 5%.

### Blood Sample Preparation for DNA Damage Focus Assay

The separation and fixation of the white blood cells and the counting of the identified DSB foci followed the protocol described in detail in Eberlein et al. (16), and the DSB foci staining was performed according to Lassmann et al. (18) and Lamkowski et al. (14). Briefly, white blood cells were obtained by density centrifugation (CPT Vacutainer tube; BD) and fixed in ice-cold 70% ethanol. Samples were kept at  $-20^{\circ}\text{C}$  until immunostaining for  $\gamma\text{-H2AX}$  and 53BP1 using primary antibodies against  $\gamma\text{-H2AX}$  (Millipore) and 53BP1 (Acris Antibodies) that were detected with secondary goat antimouse Alexa-488 and donkey antirabbit Cy3-labeled antibodies (both Dianova), respectively. The number of DSB repair protein foci was analyzed by an experienced investigator (HS) in lymphocyte nuclei ( $n = 100$  peripheral blood lymphocytes/sample) by manual focus counting using a red/green double-band pass filter (AHF) and 63 $\times$  lens of a Zeiss Axioimager 2i fluorescence microscope equipped with the ISIS fluorescence imaging system (MetaSystems).

Counting the blood sample before therapy gave us the baseline background foci rate. This rate was subtracted from the DNA foci counts obtained after irradiation, which resulted in the average number of RIF/cell.

### Measurement of Whole-Body Retention

Whole-body activity retention was determined in all patients by external dose rate measurements according to the methodology described by the EANM SOP for patients with DTC (3). Dose-rate measurements were performed by use of a ceiling-mounted shielded survey meter (automess GmbH) at a fixed distance of 2.5 m above the patients' beds. The first patient measurement was performed approximately 15 min after  $^{131}\text{I}$  application and at least 2 times per day thereafter. Data were normalized to the first measurement.

### Calculation of Time-Integrated Activity Coefficients and Absorbed Doses

The calculation of the time-dependent time-integrated activity coefficients for the total body (tb) ( $\tau_{\text{tb}}(t)$ ) and the blood (bl) ( $\tau_{\text{mL of bl}}(t)$ ) and the absorbed doses ( $\bar{D}_{\text{bl}}(t)$ ) after administration of  $^{131}\text{I}$  were performed according to the EANM SOP (3) and as described previously (16). These coefficients are obtained by integrating the respective time–activity curve from 0 to the time point  $t$  (instead of infinity). Because we took multiple blood samples and measured the retention of the whole body up to 168 h after therapy, the corresponding time–activity curves for  $^{131}\text{I}$  were fitted by bi- or triexponential functions.

Because the activity was administered orally, the iodine washout from the stomach to the blood circulation needs to be considered. According to Leggett (21) the iodine uptake is 5% per minute. Therefore, we assumed a linear iodine uptake within the first 20 min for the time–activity curve of the blood, and the bi- or triexponential fits were performed from  $t = 20$  min. The absorbed dose  $\bar{D}_{\text{bl}}(t)$  after 20 min was calculated as follows:

$$\bar{D}_{\text{bl}}(t) = A_0 \times \left( 108 \frac{\text{Gy} \cdot \text{mL}}{\text{GBq} \cdot \text{h}} \times \tau_{\text{mL of bl}}(t) + \frac{0.0188 \text{ Gy} \cdot \text{kg}^{2/3}}{wt^{2/3}} \frac{\text{Gy} \cdot \text{kg}^{2/3}}{\text{GBq} \cdot \text{h}} \times \tau_{\text{tb}}(t) \right). \quad \text{Eq. 1}$$

$A_0$  denotes the administered activity, and  $wt$  represents the patient's weight in kg.

### Modeling Time-Dependency of Focus Induction and Disappearance

The modeling of the time-dependency of the DSB focus induction and disappearance followed the method described previously (16). The number of RIF/cell as a function of the time-dependent absorbed dose and the disappearance of the foci are described in the early hours of treatment by a linear dose-dependent increase, with the parameters taken from our in vitro calibration curve (15) and a biexponential decay representing DNA repair:

$$N(t) = (a + m \times b \times \bar{D}_{\text{bl}}(t)) \times (k \times e^{-\lambda \times t} + (1 - k) \times e^{-\nu \times t}). \quad \text{Eq. 2}$$

$N(t)$  is the number of RIF/cell at time  $t$ .  $a, b$  are constants taken from the in vitro calibration curve (15); they describe the number of RIF/cell as a linear function of the time-dependent mean absorbed dose  $\bar{D}_{\text{bl}}(t)$  ( $a = 0.0363$  RIF/cell;  $b = 0.00147$  RIF/cell·mGy $^{-1}$ ). The in vitro calibration curve was generated with blood samples of volunteers who were irradiated internally with  $^{131}\text{I}$  and  $^{177}\text{Lu}$  with absorbed doses up to 100 mGy. The number of RIF/cell increased linearly with the absorbed dose to the blood.

$M$  is the adjustable parameter to account for the variability in the patient dosimetry with respect to the linear in vitro calibration function (15),  $k$  is the adjustable parameter describing the fraction of damage assigned to different repair rates, and  $\lambda$  and  $\nu$  are the patient-specific adjustable parameters describing the decay rate of foci.

### Statistics

Origin (version 9.1G+2015G; Origin Lab Corp.) was used for data analysis and statistical evaluation. Normal distribution of the datasets was tested using the Shapiro–Wilk test. Changes in RIF/cell value sets at different time points were compared by the paired Wilcoxon signed-rank test. Differences were considered to be significant if the  $P$  value was less than 0.05.

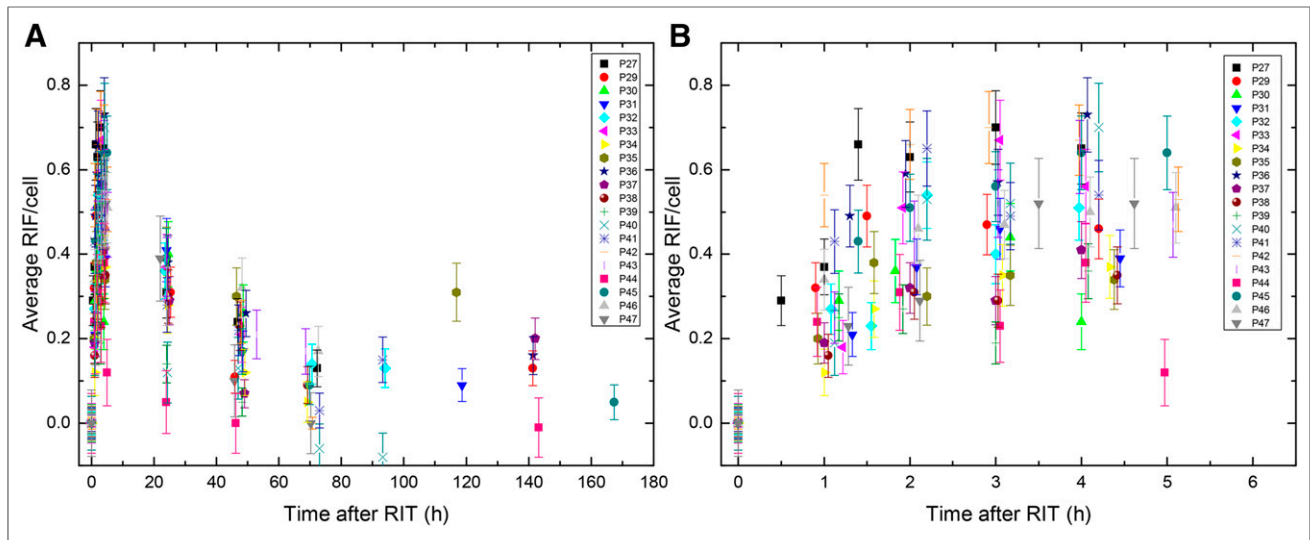


**FIGURE 1.** Average RIF/cell as function of time after administration of  $^{131}\text{I}$  for time points 0–168 h (A) and detailed view of time points 0–5 h (B).

**TABLE 1**  
Number of RIF/Cell and Absorbed Doses to Blood at Different Time Points

| Patient no. | Background foci values | Time, 4 h*          |                    | Time, 24 h*         |                    | Time, 48 h*         |                    | Total absorbed dose(mGy) |
|-------------|------------------------|---------------------|--------------------|---------------------|--------------------|---------------------|--------------------|--------------------------|
|             |                        | Absorbed dose (mGy) | No. of RIF/cell    | Absorbed dose (mGy) | No. of RIF/cell    | Absorbed Dose (mGy) | No. of RIF/cell    |                          |
| P27         | 0.024                  | 98                  | 0.650              | 284                 | 0.310              | 344                 | 0.240              | 366                      |
| P29         | 0.020                  | 52                  | 0.460              | 139                 | 0.310              | 169                 | 0.110              | 299                      |
| P30         | 0.045                  | 53                  | 0.240              | 208                 | 0.400              | 331                 | 0.260              | 594                      |
| P31         | 0.024                  | 51                  | 0.390              | 163                 | 0.410              | 203                 | 0.170              | 370                      |
| P32         | 0.028                  | 72                  | 0.510              | 252                 | 0.360              | 340                 | —                  | 429                      |
| P33         | 0.047                  | 98                  | 0.560              | 270                 | 0.370              | 328                 | 0.210              | 350                      |
| P34         | 0.042                  | 61                  | 0.370              | 199                 | 0.280              | 262                 | 0.120              | 301                      |
| P35         | 0.040                  | 59                  | 0.340              | 149                 | 0.390              | 203                 | 0.300              | 665                      |
| P36         | 0.020                  | 69                  | 0.730              | 225                 | 0.380              | 272                 | 0.260              | 315                      |
| P37         | 0.020                  | 55                  | 0.410              | 186                 | 0.290              | 231                 | 0.070              | 340                      |
| P38         | 0.032                  | 56                  | 0.350              | 195                 | 0.300              | 269                 | 0.230              | 322                      |
| P39         | 0.024                  | 60                  | 0.360              | 156                 | 0.140              | 207                 | 0.050              | 256                      |
| P40         | 0.063                  | 69                  | 0.700              | 208                 | 0.120              | 254                 | 0.130              | 420                      |
| P41         | 0.037                  | 86                  | 0.540              | 265                 | 0.280              | 347                 | 0.220              | 401                      |
| P42         | 0.014                  | 79                  | 0.670              | 214                 | —                  | 263                 | 0.240              | 285                      |
| P43         | 0.035                  | 92                  | 0.630              | 286                 | 0.370              | 363                 | 0.210              | 418                      |
| P44         | 0.071                  | 57                  | 0.380              | 192                 | 0.050              | 230                 | 0.000              | 269                      |
| P45         | 0.035                  | 63                  | 0.640              | 205                 | 0.390              | 264                 | 0.170              | 380                      |
| P46         | 0.042                  | 37                  | 0.500              | 112                 | 0.300              | 138                 | 0.320              | 275                      |
| P47         | 0.079                  | 56                  | 0.520              | 183                 | 0.390              | 247                 | 0.100              | 286                      |
| Mean        | 0.037                  | 66                  | 0.498 <sup>†</sup> | 205                 | 0.307 <sup>†</sup> | 263                 | 0.179 <sup>†</sup> | 367                      |
| SD          | 0.004                  | 17                  | 0.137              | 49                  | 0.099              | 63                  | 0.085              | 105                      |

\*Nominal time points, SD (standard deviation).

<sup>†</sup>Statistically significant differences ( $P < 0.008$ ).

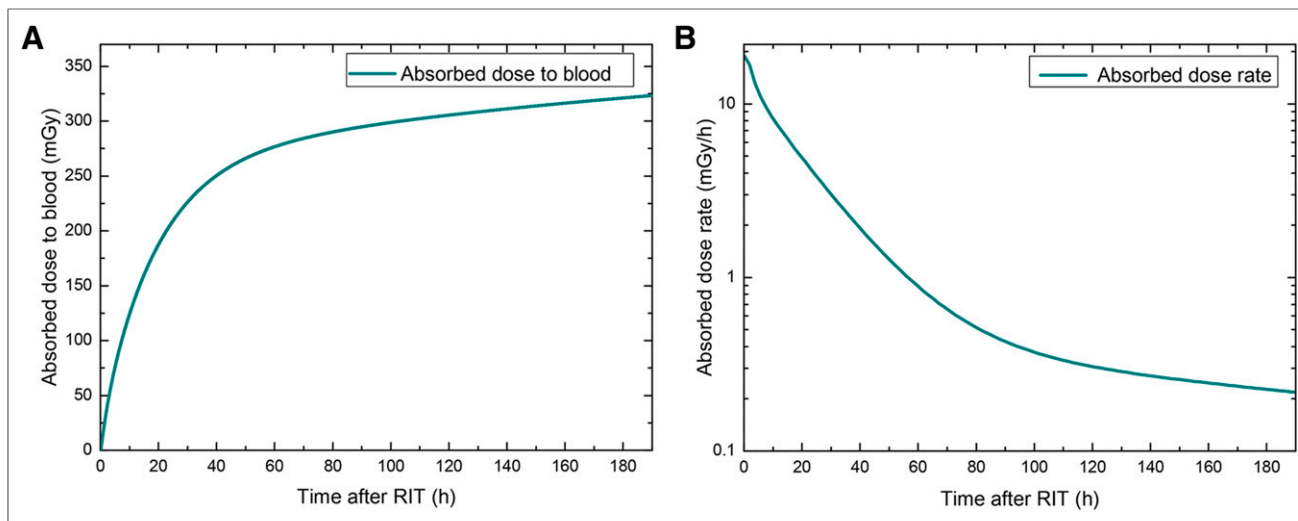


**FIGURE 2.** Absorbed dose (A) and dose rate (B) to blood for patient 45 as function of time.

## RESULTS

### Patients

Twenty patients (8 men and 12 women) with a mean age ( $\pm$ SD) of  $55.1 \pm 17.1$  y were recruited and included in this study. More details on the patients' demographics are given in Supplemental Table 1 (supplemental materials are available at <http://jnm.snmjournals.org>). Most of the patients ( $n = 16$ ) presented with papillary thyroid cancer. The patients received a mean of  $3.5 \pm 0.3$  GBq of  $^{131}\text{I}$ -iodide for their first therapy. All patients except 1 (patient 35) were treated while being hypothyroid.

Thereafter, patients were admitted to our ward and hospitalized for at least 3 d (15 patients) until the external dose rate dropped below  $3.5 \mu\text{Sv/h}$  at a distance of 2.5 m during their hospital stay. Most of the blood samples and measurements were taken during this time period. For some patients, final blood withdrawal and dose rate measurements were performed when they were scheduled for their final post-therapeutic gamma camera imaging. All patients responded well to the treatment or showed disease stabilization at follow-up. No therapy or study-related adverse events were observed.

### DNA Damage Foci

Peripheral blood lymphocytes were stained immunofluorescently for  $\gamma\text{-H2AX}$  and 53BP1 (14,18). DNA damage foci were manually enumerated for colocalizing  $\gamma\text{-H2AX}/53\text{BP1}$  DSB-marking foci. Average numbers of RIF/cell were calculated for each patient sample (Fig. 1) as a function of time after administration of the radiopharmaceutical. The average number of RIF/cell increased in the first hours after therapy, declining at later time points (Fig. 1; Table 1). The actual time points differed slightly because of variations in the individual patient management. The mean number of foci varied between  $0.50 \pm 0.14$  RIF/cell at 4 h,  $0.31 \pm 0.10$  RIF/cell at 24 h, and  $0.18 \pm 0.09$  RIF/cell at 48 h after administration of  $^{131}\text{I}$ .

Only datasets of 4 and 48 h were distributed according to a gaussian distribution (Shapiro–Wilk test). Therefore, we chose a nonparametric test (Wilcoxon signed-rank test) to compare the datasets at 4, 24, and 48 h. Application of the Wilcoxon signed-rank test to those time points revealed that there was a statistically significant decrease between the number of RIF/cell at these time

points ( $P < 0.05$ ), confirming the observation that the number of RIF/cell declined 5 h after administration of the radiopharmaceutical (Fig. 1).

### Dosimetry

The absorbed doses to the blood for the individual patients were calculated according to the EANM SOP (3). The mean absorbed dose was  $66 \pm 17$  mGy at 4 h,  $205 \pm 49$  mGy after 24 h, and  $263 \pm 63$  mGy after 48 h, and the total absorbed dose after administration was  $367 \pm 105$  mGy (Table 1). The specific total absorbed dose to the blood in all hypothyroid patients was  $100 \pm 22$  mGy/GBq. This value is in good agreement with the value of  $93 \pm 35$  mGy/GBq found in our previous study (18), further confirming the validity of the method.

The absorbed dose to the blood increased steeply in the first few hours after therapy (Fig. 2A). In most patients, 50% of the total

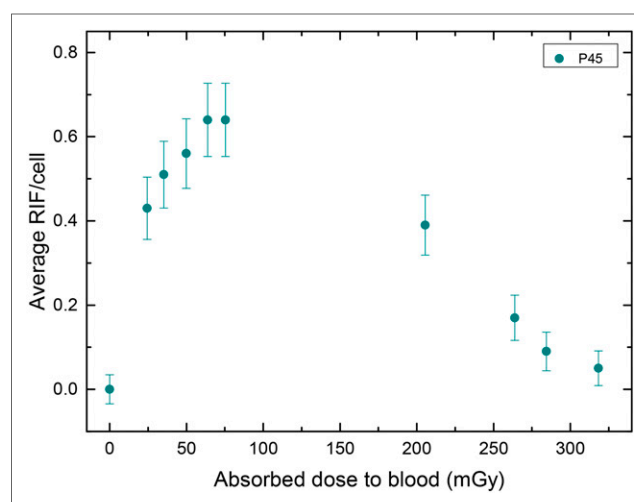


**FIGURE 3.** Average RIF/cell as function of absorbed dose to blood for patient 45. Time points of blood withdrawals were 0, 1.4, 2.0, 3.0, 4.0, 5.0, 24.0, 48.2, 69.8, and 167.3 h.

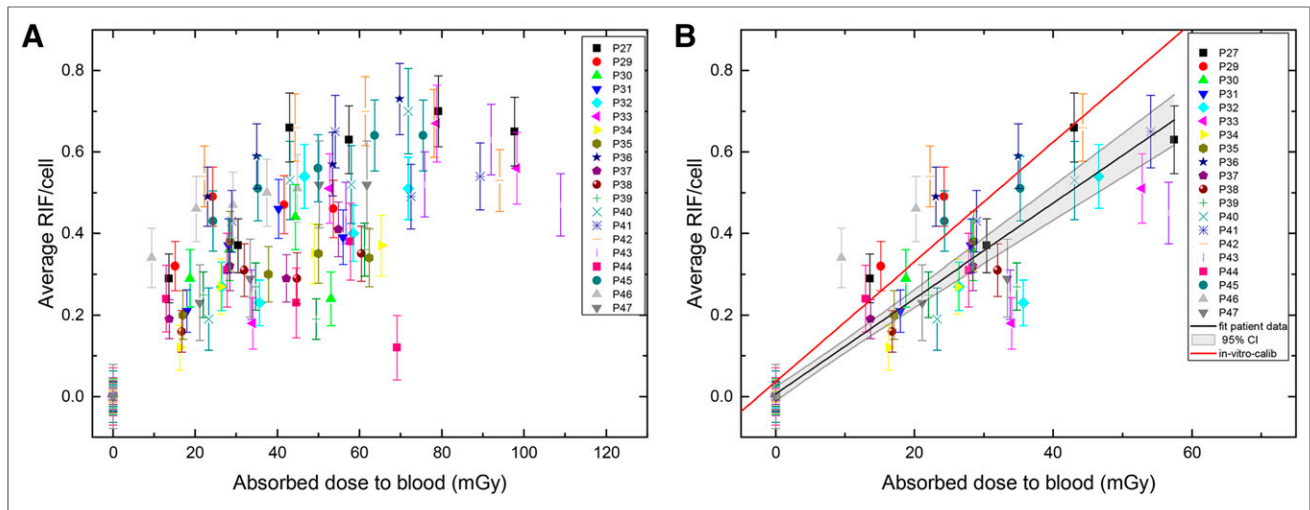


**FIGURE 4.** Average number of RIF/cell as a function of the absorbed dose to blood for the first 5 h (A) and for the first 2 h (B) after  $^{131}\text{I}$  administration. The black line is a linear fit to our  $^{131}\text{I}$  patient data including a 95% confidence interval (CI), and the red line is the in vitro calibration curve taken from Eberlein et al. (15).

absorbed dose to the blood was reached within the first 24 h (Fig. 2B). In accordance with this observation, the dose rate declined until it was 0.5 mGy/h or less after 80 h. For overview, Figure 3

shows the average RIF/cell values of an exemplary patient (patient 45) as a function of the absorbed dose to the blood.

**TABLE 2**

Individual Fit Parameters for Equation 2

| Patient no.               | m     | $\lambda \text{ h}^{-1}$ | k     | $\nu \text{ h}^{-1}$ |
|---------------------------|-------|--------------------------|-------|----------------------|
| P27                       | 1.010 | 0.284                    | 0.883 | 0.034                |
| P29                       | 1.868 | 0.659                    | 0.723 | 0.080                |
| P30*                      | 0.338 | 0.058                    | 1     | —                    |
| P31                       | 1.050 | 0.414                    | 0.520 | 0.058                |
| P32                       | 0.750 | 0.207                    | 0.782 | 0.035                |
| P33*                      | 0.524 | 0.072                    | 1     | —                    |
| P34                       | 0.657 | 0.215                    | 0.542 | 0.051                |
| P35                       | 0.949 | 0.365                    | 0.825 | 0.010                |
| P36                       | 1.027 | 0.281                    | 0.945 | 0.015                |
| P37†                      | 0.639 | 0.083                    | 1     | —                    |
| P38                       | 0.728 | 0.260                    | 0.673 | 0.036                |
| P39*                      | 0.461 | 0.098                    | 1     | —                    |
| P40, fit did not converge |       |                          |       |                      |
| P41                       | 1.254 | 0.428                    | 0.837 | 0.056                |
| P42, fit did not converge |       |                          |       |                      |
| P43                       | 0.566 | 0.153                    | 0.790 | 0.026                |
| P44, fit did not converge |       |                          |       |                      |
| P45                       | 1.335 | 0.301                    | 0.683 | 0.056                |
| P46                       | 2.504 | 0.336                    | 0.896 | 0.020                |
| P47†                      | 0.875 | 0.076                    | 1     | —                    |
| Mean                      | 1.101 | 0.325                    | 0.758 | 0.040                |
| SD                        | 0.532 | 0.128                    | 0.129 | 0.020                |
| Median                    | 1.019 | 0.293                    | 0.786 | 0.036                |

\*Latest time point: 48 h.

†For these patients, a monoexponential function described RIF/cell data best.

### In Vivo Calibration of DNA Damage Focus Assay

A fit within the first 4–5 h, as performed in the publication with  $^{177}\text{Lu}$  patients (16), after administration of the radioactivity could not be performed. The reason was the observation of a slower increase of the number of RIF/cell after 2 h. For the in vivo calibration, therefore, only the first 2 h after administration of the radioactivity or the first 2 data points were considered. Those datasets were pooled, and the average number of RIF/cell as a function of the absorbed dose was fitted linearly:

$$y = 0.0064 \times \text{RIF/cell} + 0.0117 \times \text{RIF/cell} \times \text{mGy}^{-1} \times x \quad (3)$$

$y$  denotes the number of RIF/cell and  $x$  the absorbed dose to the blood in mGy ( $R^2 = 0.86$ ). The SE of the  $y$ -axis intercept is  $\pm 0.0089$  RIF/cell, and the SE of the slope is  $\pm 0.0006$  RIF/cell  $\text{mGy}^{-1}$ . The resulting in vivo calibration curve for our experiments including a 95% confidence interval is shown in Figure 4 as a black line.

In a previous study, we obtained an in vitro calibration in blood samples of volunteers for  $^{131}\text{I}$  and  $^{177}\text{Lu}$  (15). For comparison, this in vitro calibration curve is shown as a red line in Figure 4. The slope for the patient data is shallower, with a relative deviation of the slopes of 20% between the in vitro calibration and the in vivo data.

Compared with the fit of the  $^{177}\text{Lu}$  patients (16), the  $^{131}\text{I}$  in vivo fit has a slope that is 7.9% lower. This is most likely caused by the early onset of a fast DNA damage repair component in the  $^{131}\text{I}$  patients.

### Modeling

Individual fits of the patient foci data after the first RIT were performed according to Equation 2 using the datasets for the biokinetics of blood and whole body. Variable parameters to be fitted were  $m$ ,  $\lambda$ ,  $k$ , and  $\nu$  (Table 2). The biexponential fit converged for 12 patients. Three patients showed a fast decay of the number of RIF/cell (patients 40, 42, and 44). For these patients, the fit did not converge. Three patients (patients 30, 33, and 39)

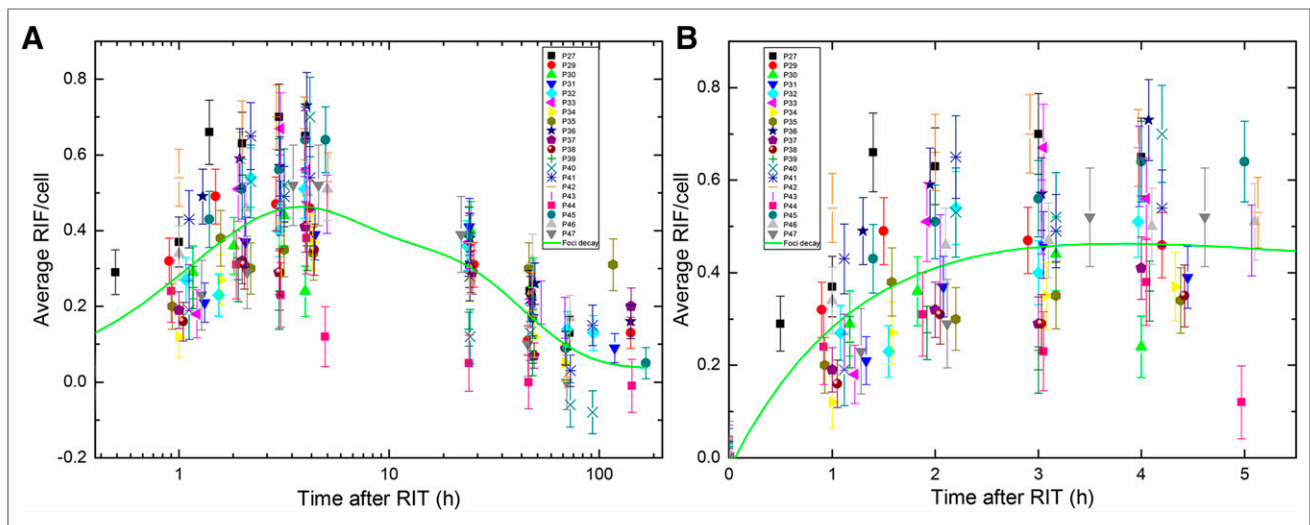


**FIGURE 5.** Average number of RIF/cell as function of time after  $^{131}\text{I}$  administration (A). The green curve represents the response function according to Equation 2 using mean values for all parameters. (B) More detailed view of the response function for the first 5 h after  $^{131}\text{I}$  administration.

were released from the ward 48 h after administration; therefore, blood samples could not be taken at later time points, and, consequently, a biexponential fit was impossible. For patients 37 and 47, a monoexponential decay represented the RIF/cell data better although their blood samples were taken at time points of 48 h or later; the mean values including their SD were taken from the 12 patients for whom the fit converged and had 3 or more data points of 24 h or more (Table 2).

In general, the data followed a straight line for the first 1–2 h after  $^{131}\text{I}$  administration. The mean value of the fit parameter  $m$ , which accounts for the variability in the patient dosimetry with respect to the *in vitro* calibration, was  $1.10 \pm 0.53$  (minimum, 0.56; maximum, 2.50). The mean (fast) decay rate ( $\lambda$ ) for all 12 patients was  $0.325 \pm 0.128 \text{ h}^{-1}$  (minimum,  $0.15 \text{ h}^{-1}$ ; maximum,  $0.66 \text{ h}^{-1}$ ). The (slow) decay rate  $\nu$  ranged from 0.01 to  $0.08 \text{ h}^{-1}$  (mean,  $0.040 \pm 0.020 \text{ h}^{-1}$ ). The mean value for  $k$  was  $0.758 \pm 0.129$ , indicating that about 76% of the DNA damage is repaired with a high decay rate. Expressed as half-lives, the mean values of the fast decay was  $T_{\text{fast}} = 2.1 \text{ h}$  and  $T_{\text{slow}} = 17.3 \text{ h}$ .

The time-dependent response function (Eq. 2) shown in Figure 5 (green curve) is based on the mean parameters provided in Table 2. According to this function, the highest number of RIF/cell can be expected 3.2 h after administration of  $^{131}\text{I}$ . After 148 h, the mean DSB foci values drop below the maximum SD of the background RIF/cell value of  $0 \pm 0.04$  RIF/cell. The SD of the background foci includes the counting error; therefore, each data point is considered with appropriate error propagation, even the baseline value of the RIF/cell at 0 mGy. This indicates that some patients still have slightly elevated numbers of RIF, even up to 4 d after treatment started.

## DISCUSSION

There still is a limited number of publications investigating the effect of DSB induction after radionuclide therapy or diagnostics (16,18–20,22). However, nuclear medicine treatments involve systemic internal irradiation as compared with external irradiation (e.g., in radiotherapy). After radionuclide incorporation, the cells are not only irradiated by internalized

and extracellular  $^{131}\text{I}$  for seconds or minutes but are continuously irradiated over a longer period with permanently changing dose rate. This could alter the effect of radiation damage compared with a fractionated high-dose-rate partial-body irradiation in radiotherapy. In a previous peptide receptor radionuclide therapy (PRRT) study with  $^{177}\text{Lu}$ , we reported a first linear relationship between the number of RIF/cell and the absorbed dose to the blood only over the first 4–5 h after therapy start (16). After this period, the disappearance of the DSB foci was reflected by the decay of the RIF/cell numbers.

This study with  $^{131}\text{I}$  showed a similar relationship; however, the time period of the linear dependence was reduced to 2 h after administration of the  $\beta$ -emitter  $^{131}\text{I}$  (Fig. 1B), indicating a faster decay of the RIF/cell number. The time points after 2 h were characterized by a diminishing number of radiation-induced foci in accordance with the progression of DNA repair and the declining dose rates. This finding agrees well with our previous studies that showed the highest value of RIF/cell at early time points, with subsequent, statistically significant reduction of the RIF/cell numbers at later time points (16,18).

Analysis of  $\gamma\text{-H2AX/53BP1}$  foci kinetics in peripheral blood lymphocytes of 16 patients undergoing PRRT (16) revealed, however, likely due to the short time period of measurement after therapy (<48 h), only a monoexponential decay curve (16). Compared with our previous study in patients after PRRT, there is a deviation from a straight line in this study at time points of  $\geq 2$  h after  $^{131}\text{I}$  administration. This might be caused by the higher mean absorbed dose imparted to the blood in the first hour after treatment ( $14 \pm 5 \text{ mGy}$  for  $^{177}\text{Lu}$  PRRT [unpublished data taken from our PRRT study],  $23 \pm 8 \text{ mGy}$  for  $^{131}\text{I}$  RIT). This effect mirrors the one for the differential foci response of human fibroblasts after irradiation with X-rays for absorbed doses greater than 10 mGy (23).

The disappearance of RIF/cell as a function of time has been quantitatively described by Horn et al. (24), Mariotti et al. (25), and Eberlein et al. (16). The values reported in this study for the slow and fast component of decay were in good agreement with the findings of Horn et al. (24), characterizing the disappearance of RIF/cell by a biexponential response function with a short decay rate of  $0.35 \text{ h}^{-1}$



(77%) and a longer-lived component of  $0.018 \text{ h}^{-1}$  (23%). The range of our RIF/cell decay rate for the fast component is within the value ranges of Horn et al. (24) and Mariotti et al. (25) ( $0.23 \text{ h}^{-1}$ ). The slow decay component by Mariotti et al. does not contribute greatly to the decay of RIF/cell (probability, 9%) and is less than  $10^{-11} \text{ h}^{-1}$ . Most likely, their way of irradiating the cells does not compare to our case of continuous internal irradiation with decreasing dose rate.

Several RIT patients showed a fast monoexponential decay rate, pointing at the fact that their DSB repair could have been more effective as compared with the other patients. However, for these patients no obvious link between this finding and the pretreatment or stage of the disease could be found.

Further studies with more patients and other isotopes/radiopharmaceuticals showing different kinetics of the tracer in the blood are needed to better identify repair kinetics and patients with different repair rates.

## CONCLUSION

This study describes the kinetics of  $^{131}\text{I}$  incorporation–induced DSBs in blood lymphocytes during radioiodine therapy as a function of the absorbed dose to the blood. In the first hours after therapy, the number of radiation-induced DSBs per cell increased linearly with the absorbed dose and mirrored our recently established in vitro calibration curve. At more advanced time points after administration of the radiopharmaceutical, the induction of a fast and a slow repair component of the double-strand DNA damage was seen. In this study, we found a dose-dependent analytic function describing the internal  $^{131}\text{I}$  irradiation–induced time course of induction and decay of DSB foci in RIT patients.

## DISCLOSURE

The costs of publication of this article were defrayed in part by the payment of page charges. Therefore, and solely to indicate this fact, this article is hereby marked “advertisement” in accordance with 18 USC section 1734. This study was funded by a grant of the Deutsche Forschungsgemeinschaft (DFG) (no. LA 2304/3-1). The funders had no role in study design, data collection and analysis, decision to publish, or preparation of the manuscript. No other potential conflict of interest relevant to this article was reported.

## ACKNOWLEDGMENTS

We thank all patients who participated in the study for their contribution. We also thank the members of the nuclear medicine team and, particularly, Inge Grelle, Heike Göbel, and Carina Novak for support and assistance.

## REFERENCES

1. Luster M, Clarke SE, Dietlein M, et al. Guidelines for radioiodine therapy of differentiated thyroid cancer. *Eur J Nucl Med Mol Imaging*. 2008;35:1941–1959.
2. American Thyroid Association (ATA) Guidelines Taskforce on Thyroid Nodules and Differentiated Thyroid Cancer, Cooper DS, Doherty GM, et al. Revised American Thyroid Association management guidelines for

- patients with thyroid nodules and differentiated thyroid cancer. *Thyroid*. 2009;19:1167–1214.
3. Lassmann M, Häscheid H, Chiesa C, Hindorf C, Flux G, Luster M. EANM Dosimetry Committee series on standard operational procedures for pre-therapeutic dosimetry I: blood and bone marrow dosimetry in differentiated thyroid cancer therapy. *Eur J Nucl Med Mol Imaging*. 2008;35:1405–1412.
4. Manning G, Rothkamm K. Deoxyribonucleic acid damage-associated biomarkers of ionising radiation: current status and future relevance for radiology and radiotherapy. *Br J Radiol*. 2013;86:20130173.
5. Rogakou EP, Pilch DR, Orr AH, Ivanova VS, Bonner WM. DNA double-stranded breaks induce histone H2AX phosphorylation on serine 139. *J Biol Chem*. 1998;273:5858–5868.
6. Rothkamm K, Löbrich M. Evidence for a lack of DNA double-strand break repair in human cells exposed to very low x-ray doses. *Proc Natl Acad Sci USA*. 2003;100:5057–5062.
7. Ivashkevich A, Redon CE, Nakamura AJ, Martin RF, Martin OA. Use of the  $\gamma$ -H2AX assay to monitor DNA damage and repair in translational cancer research. *Cancer Lett*. 2012;327:123–133.
8. Schultz LB, Chehab NH, Malikzay A, Halazonetis TD. p53 binding protein 1 (53BP1) is an early participant in the cellular response to DNA double-strand breaks. *J Cell Biol*. 2000;151:1381–1390.
9. Anderson L, Henderson C, Adachi Y. Phosphorylation and rapid relocalization of 53BP1 to nuclear foci upon DNA damage. *Mol Cell Biol*. 2001;21:1719–1729.
10. Rappold I, Iwabuchi K, Date T, Chen J. Tumor suppressor p53 binding protein 1 (53BP1) is involved in DNA damage-signaling pathways. *J Cell Biol*. 2001;153:613–620.
11. Huyen Y, Zgheib O, DiTullio RA Jr, et al. Methylated lysine 79 of histone H3 targets 53BP1 to DNA double-strand breaks. *Nature*. 2004;432:406–411.
12. Panier S, Boulton SJ. Double-strand break repair: 53BP1 comes into focus. *Nat Rev Mol Cell Biol*. 2014;15:7–18.
13. Ward IM, Minn K, Jorda KG, Chen J. Accumulation of checkpoint protein 53BP1 at DNA breaks involves its binding to phosphorylated histone H2AX. *J Biol Chem*. 2003;278:19579–19582.
14. Lamkowski A, Forcherson F, Agay D, et al. DNA Damage focus analysis in blood samples of minipigs reveals acute partial body irradiation. *PLoS One*. 2014;9:e87458.
15. Eberlein U, Peper M, Fernández M, Lassmann M, Scherthan H. Calibration of the  $\gamma$ -H2AX DNA double strand break focus assay for internal radiation exposure of blood lymphocytes. *PLoS One*. 2015;10:e0123174.
16. Eberlein U, Nowak C, Bluemel C, et al. DNA Damage in blood lymphocytes in patients after Lu-177 peptide receptor radionuclide therapy. *Eur J Nucl Med Mol Imaging*. 2015;42:1739–1749.
17. Chowdhury D, Keogh M-C, Ishii H, Peterson CL, Buratowski S, Lieberman J.  $\gamma$ -H2AX dephosphorylation by protein phosphatase 2A facilitates DNA double-strand break repair. *Mol Cell*. 2005;20:801–809.
18. Lassmann M, Häscheid H, Gassen D, et al. In vivo formation of  $\gamma$ -H2AX and 53BP1 DNA repair foci in blood cells after radioiodine therapy of differentiated thyroid cancer. *J Nucl Med*. 2010;51:1318–1325.
19. Doai M, Watanabe N, Takahashi T, et al. Sensitive immunodetection of radio-toxicity after iodine-131 therapy for thyroid cancer using  $\gamma$ -H2AX foci of DNA damage in lymphocytes. *Ann Nucl Med*. 2013;27:233–238.
20. Denoyer D, Lobachevsky P, Jackson P, Thompson M, Martin OA, Hicks RJ. Analysis of  $^{177}\text{Lu}$ -octreotate therapy–induced DNA damage in peripheral blood lymphocytes of patients with neuroendocrine tumors. *J Nucl Med*. 2015;56:505–511.
21. Leggett RW. A physiological systems model for iodine for use in radiation protection. *Radiat Res*. 2010;174:496–516.
22. May MS, Brand M, Wuest W, et al. Induction and repair of DNA double-strand breaks in blood lymphocytes of patients undergoing  $^{18}\text{F}$ -FDG PET/CT examinations. *Eur J Nucl Med Mol Imaging*. 2012;39:1712–1719.
23. Grudzenski S, Raths A, Conrad S, Rube CE, Löbrich M. Inducible response required for repair of low-dose radiation damage in human fibroblasts. *Proc Natl Acad Sci USA*. 2010;107:14205–14210.
24. Horn S, Barnard S, Rothkamm K. Gamma-H2AX-based dose estimation for whole and partial body radiation exposure. *PLoS One*. 2011;6:e25113.
25. Mariotti LG, Pirovano G, Savage KI, et al. Use of the  $\gamma$ -H2AX assay to investigate DNA repair dynamics following multiple radiation exposures. *PLoS One*. 2013;8:e79541.